## TITLE

# CDPK2A and CDPK1 form a signaling module upstream of *Toxoplasma* motility


## AUTHORS

Emily Shortt[a], Caroline G. Hackett[a]*, Rachel V. Stadler[b], Gary E. Ward[b], Sebastian Lourido[a,c#]

[a] Whitehead Institute, Cambridge, MA

[b] Department of Microbiology and Molecular Genetics, University of Vermont Larner College of Medicine, Burlington, VT

[c] Biology Department, MIT, Cambridge, MA

* Current address: Regeneron Pharmaceuticals, Tarrytown, NY

[#] Correspondence: lourido@wi.mit.edu


## RUNNING TITLE

CDPK2A works with CDPK1 to regulate *T. gondii* motility


## ABSTRACT

The transition between parasite replication and dissemination is regulated in apicomplexan parasites by fluctuations in cytosolic calcium concentrations, effectuated by calcium-dependent protein kinases (CDPKs). We examined the role of CDPK2A in the lytic cycle of *Toxoplasma*, analyzing its role in the regulation of cellular processes associated with parasite motility. We used chemical-genetic approaches and conditional depletion to determine that CDPK2A contributes to the initiation of parasite motility through microneme discharge. We demonstrate that the N-terminal extension of CDPK2A is necessary for the protein's function. Conditional depletion revealed an epistatic interaction between CDPK2A and CDPK1, suggesting that the two kinases work together to mediate motility in response to certain stimuli. This signaling module appears distinct from that of CDPK3 and PKG, which also controls egress. CDPK2A is revealed as an important regulator of the *Toxoplasma* kinetic phase, linked to other kinases that govern this critical transition. Our work uncovers extensive interconnectedness between the signaling pathways that govern parasite motility.


## IMPORTANCE

This work uncovers interactions between various signaling pathways that govern *Toxoplasma gondii* egress. Specifically, we compare the function of three canonical calcium dependent protein kinases (CDPKs) using chemical-genetic and conditional-depletion approaches. We describe the function of a previously uncharacterized CDPK, CDPK2A, in the *Toxoplasma* lytic cycle, demonstrating it contributes to parasite fitness through regulation of microneme discharge, gliding motility, and egress from infected host cells. Comparison of analog-sensitive (AS) kinase alleles and conditionally-depleted alleles uncovered epistasis between CDPK2A and CDPK1 implying a partial functional redundancy.

Understanding the topology of signaling pathways underlying key events in the parasite life cycle can aid in efforts targeting parasite kinases for anti-parasitic therapies.

## INTRODUCTION

Apicomplexan pathogens like *Toxoplasma gondii*, *Plasmodium* spp., and *Cryptosporidium* spp. sense and adapt to changes in the host environment throughout their life cycles. These transitions between states often require rapid cellular responses, for which calcium ions ($Ca^{2+}$) are well suited as second messengers. Cells maintain low $Ca^{2+}$ concentrations in the cytosol, in stark contrast to the extracellular milieu and the lumen of some organelles (1). Increased membrane permeability can therefore quickly change the cytosolic $Ca^{2+}$ concentration and initiate signaling. In apicomplexans, such signaling controls progression through the lytic cycle.

The *Toxoplasma* lytic cycle comprises two main phases: a replicative phase during which parasites divide in a parasitophorous vacuole and a kinetic phase that includes egress from the infected host cell, gliding motility, and active invasion of a new host cell. $Ca^{2+}$ signaling mediates the transition between the replicative and kinetic phases of the lytic cycle. After several rounds of replication, parasites actively disrupt surrounding membranes and move out of the infected cell in a process termed egress. This process can be artificially triggered through the use of $Ca^{2+}$ ionophores like ionomycin and A23187 (2–5). $Ca^{2+}$ fluxes can be observed with fluorescent dyes and genetically encoded reporters, which show $Ca^{2+}$ surges that precede gliding motility and invasion in *Toxoplasma (5–7)*. $Ca^{2+}$ oscillations also occur throughout the *Plasmodium* lytic cycle, with peaks in $Ca^{2+}$ concentration preceding microneme secretion, invasion, gliding, and egress (8–11). Control of cytosolic $Ca^{2+}$ concentrations is therefore critical for the regulation of the parasite lytic cycle.

Cytosolic $Ca^{2+}$ surges originate from the release of intracellular stores or by crossing the plasma membrane (PM) from the extracellular space (12, 13). In *T. gondii*, intracellular stores include the endoplasmic reticulum (ER), acidocalcisomes, and plant-like vacuole—with the ER or a related compartment representing the most likely sources of $Ca^{2+}$ during signaling (14). The channels responsible for $Ca^{2+}$ release have yet to be identified in apicomplexans; however, stimulation of the cGMP signaling pathway triggers this process in *T. gondii* and *Plasmodium* spp. (7, 15–17). Treatment with the phosphodiesterase inhibitors zaprinast and BIPPO can block hydrolysis of cGMP and trigger egress (18–20) through the release of intracellular $Ca^{2+}$ stores (7, 15–17). Protein Kinase G (PKG) is a key mediator of $Ca^{2+}$ release, presumably through activation of phosphoinositide signaling, whereby phosphatidylinositol 4,5-bisphosphate ($PIP_2$) is hydrolyzed by phosphoinositide phospholipase C (PI-PLC) into inositol triphosphate ($IP_3$) and diacylglycerol (DAG). This represents a potential branch point in the signaling pathway, with $IP_3$ triggering release of intracellular $Ca^{2+}$ stores through an undefined channel, while DAG is converted into phosphatidic acid (PA) and independently contributes to the kinetic phase (21). Parasite motility therefore requires active cGMP and $Ca^{2+}$ pathways, consistent with the observation that stimulation by $Ca^{2+}$ ionophores cannot overcome the inhibition of PKG in the context of egress (19).

Many $Ca^{2+}$-mediated phenotypes can be attributed to the $Ca^{2+}$-dependent discharge of micronemes, which are specialized organelles that contain adhesins necessary for gliding motility (22, 23). While

synthetic treatments like ionophores or phosphodiesterase inhibitors can artificially raise cytosolic $Ca^{2+}$ concentrations and trigger microneme discharge, studies suggest that serum albumin may be a natural agonist of this process (16). The single-pass transmembrane protein MIC2 is a prototypical adhesin that has been used to monitor *T. gondii* microneme discharge. Following its release, MIC2 can be engaged by the actomyosin machinery for gliding motility (12, 24, 25). Several proteases rapidly shed the ectodomain of MIC2 from the surface of the parasite, so its presence in supernatants can be used as a measure of microneme discharge (24). The *P. falciparum* ortholog of MIC2, TRAP, is required for sporozoite motility and invasion (26), and several other adhesins are similarly released and processed in both *Toxoplasma* and *Plasmodium (24, 27, 28)*. *T. gondii* micronemes additionally contain the pore-forming protein PLP1, which permeabilizes the parasitophorous vacuole membrane (PVM) and host PM during egress (29). Following membrane disruption, parasites employ gliding motility to ultimately escape from the ruptured vacuole (25, 30). Perforin-like proteins are also required for egress of *P. falciparum* and *P. berghei* merozoites and gametocytes (31–33). Although the repertoire of microneme proteins differs between species, the $Ca^{2+}$-dependent discharge and participation in gliding motility appear conserved across the phylum (34–36).

$Ca^{2+}$ regulates several cellular processes besides microneme discharge, as evidenced by the wide array of proteins that respond directly to $Ca^{2+}$ concentrations through changes in conformation, stability, localization, or interactions (14). Specialized domains, such as EF hands and C2 domains, endow proteins with the ability to alter their conformation in response to $Ca^{2+}$ binding. Apicomplexans encode several EF hand–containing proteins including calmodulins (CaMs), calcineurin B, and calcium-dependent protein kinases (CDPKs). CDPKs are critical components of the $Ca^{2+}$ signaling network due to their ability to directly respond to $Ca^{2+}$ and phosphorylate other proteins. Although initially identified in plants, CDPKs were later found in ciliates and apicomplexans (14). Despite their similarity to $Ca^{2+}$/CaM–dependent protein kinases, CDPKs are absent from mammals (37). Canonical CDPKs have four C-terminal calmodulin-like EF hands acting as the calcium-binding domain, linked by an autoinhibitory domain to the kinase domain (37, 38). CDPKs in plants control responses to a broad array of stresses, extent of starch accumulation, cell morphology, and viability. Plant CDPKs are expressed across a variety of tissue types and with various subcellular localizations (38). CDPKs exhibit a wide range of affinities for $Ca^{2+}$. For example, soybean CDPKα is activated by ten times lower $Ca^{2+}$ concentrations than CDPKγ (39, 40). Different CDPKs may therefore be tuned to respond to $Ca^{2+}$ spikes of varying magnitudes leading to variable downstream effects that may be further refined by subcellular localization. The array of apicomplexan CDPKs may analogously contribute to the magnitude and compartmentalization of $Ca^{2+}$ responses.

CDPKs are overrepresented in apicomplexan genomes. There are six canonical CDPKs in *T. gondii*, which can be further categorized by having short or long N-terminal extensions (37). Myristoylation sites cap the short extensions of CDPK1 and CDPK3, with an additional palmitoylation site localizing CDPK3 to the parasite PM (19, 41). By contrast, the purpose of the N-terminal extensions remains unknown. A further nine CDPKs in *T. gondii* display non-canonical configurations, with varying numbers and arrangements of EF hands and additional domains (37, 42). The function of most non-canonical CDPKs remains obscure in *T. gondii (42)*, with the exception of CDPK7, which has been implicated in parasite cell division and is critical for phospholipid synthesis and vesicular trafficking (43, 44). By

contrast, several canonical CDPKs are required for specific life cycle stages in apicomplexans. In *Plasmodium* spp., several CDPKs regulate specific steps of sexual differentiation (45, 46). CDPKs are also important for kinetic-phase phenotypes in *Toxoplasma* and *Plasmodium*, including microneme discharge, gliding motility, invasion, and egress. TgCDPK1 and TgCDPK3 control *Toxoplasma* egress downstream of PKG (19, 41, 47), analogously to PfCDPK5 in *Plasmodium (10, 48)*. In *Toxoplasma,* CDPK1 is required for invasion as well as egress (19, 47), potentially due to its regulation of microneme secretion under a broader array of conditions than CDPK3. Altogether, CDPKs have been revealed as essential components of the $Ca^{2+}$ signaling network, although the functions of many individual kinases remain unexplored.

In reviewing the results of a genome-wide essentiality screen, most canonical CDPKs were dispensable in tachyzoites; however, CDPK2A remained uncharacterized despite its impact on parasite fitness (49). We sought to characterize the function of CDPK2A within the lytic cycle, comparing its role to that of CDPK1 and CDPK3, two previously-described regulators of the kinetic phase. By turning to a combination of chemical and genetic manipulations we uncover significant interconnectedness between the relevant pathways. Our efforts start to discern the contribution of the various components to the cellular pathways that control microneme discharge, motility, and egress.

## RESULTS

### Chemical-genetic analysis of CDPK2A demonstrates it is involved in parasite egress

To identify the CDPKs that are necessary during the parasite lytic cycle, we examined the results of a genome-wide knockout screen that measured the relative contribution of each gene to fitness as parasites replicated in human fibroblasts (49). Most canonical CDPKs were dispensable in this analysis, including the previously-studied CDPK3; however, CDPK1 and CDPK2A were fitness-conferring, indicated by phenotype scores of -3.3 and -2.05, respectively (**Fig. 1A**). Of these potentially-essential CDPKs, the function of CDPK2A has not been previously examined. Studies of CDPK1 and CDPK3 used analog-sensitive kinase alleles, in which the gatekeeper residue of the ATP-binding pocket of the kinase of interest is mutated to Gly, yielding a binding pocket that accommodates bulky ATP-analog inhibitors (also known as bumped kinase inhibitors), such as 3-MB-PP1 (**Fig. 1B**) (50–52). CDPK1 has a naturally-occurring Gly gatekeeper and can be rendered resistant to 3-MB-PP1 inhibition through mutation of the gatekeeper residue to Met—the same residue that renders CDPK3 and CDPK2A naturally resistant to the inhibitor (50, 51). Comparison of analog-sensitive and insensitive alleles can be used to isolate the effect of inhibiting the kinase in question. Using this approach, CDPK1 was shown to control parasites' ability to perform gliding motility, invade, and egress from host cells (47). By contrast, compound-mediated inhibition of CDPK3 was used to determine its contribution to motility and egress in response to specific agonists, but not invasion (19), corroborating genetic studies (41, 53).

Given the apparent fitness contribution of CDPK2A, we sought to examine its role in the *Toxoplasma* lytic cycle through the use of analog-sensitive alleles. In a strain harboring a 3-MB-PP1–resistant, myc-tagged CDPK1 allele ($CDPK1^{M}$) (19), we modified the CDPK2A locus to introduce a C-terminal Ty epitope tag and either a Met or Gly gatekeeper residue (**Fig. 1C**). The Met modification ($CDPK2A^{M}$) retains the natural resistance of CDPK2A to 3-MB-PP1, whereas the Gly modification ($CDPK2A^{G}$)

renders the kinase 3-MB-PP1-sensitive. We confirmed the presence of the mutated gatekeeper residues by allele-specific PCR (**Fig. S1A**) and the expression of the Ty-tagged CDPK2A alleles by immunoblot (**Fig. 1D**). Construction of the isogenic strains carrying alleles of CDPK2A with different susceptibilities to bumped kinase inhibitors allowed us to examine the effect of kinase inhibition on various steps within the lytic cycle.

Parasites can be stimulated to egress from host cells by treating cultures with the calcium ionophore A23187(2) or phosphodiesterase inhibitors such as zaprinast (19) or BIPPO (18). Different agonists have been used to identify pathway-specific requirements for certain kinases (19, 54). Egress leads to loss of host-cell integrity, which can be assayed quantitatively and kinetically as the incorporation of the fluorescent dye 4′,6-diamidino-2-phenylindole (DAPI) into the nuclei of permeabilized cells (55). We compared the impact of inhibiting CDPK1, CDPK3, or CDPK2A on A23187-stimulated egress. All three kinases appeared to be required for egress under these conditions. Inhibition of either $CDPK1^{G}$ or $CDPK3^{G}$ strains reduced egress by 66% and 84% compared to vehicle treatment, in agreement with previous findings (19, 41, 47, 53). Analogously, inhibition of $CDPK2A^{G}$ decreased egress by 61% compared to vehicle treatment (**Fig. 1E–F**). Importantly, parasites expressing the resistant allele ($CDPK2A^{M}$) egressed normally in the presence of 3-MB-PP1. To compare the rates of egress, we determined the time required for each strain to achieve half of the maximum egress observed for the respective vehicle-treated control ($T_{half\text{-}max}$). Inhibition of all three kinases prevented parasites from reaching half of the maximum egress during the 10-minute observation period (denoted as $T_{half\text{-}max}$ > 600 s; **Fig. S1B**). To ensure that the effects observed were the result of differences in egress and not multiplicity of infection, we verified that monolayers had equivalent numbers of parasite vacuoles (**Fig. S1C**). Taken together, these results suggest that CDPK2A contributes to egress, along with CDPK1 and CDPK3.

We next assessed the contribution of CDPK2A to parasite egress after treatment with the phosphodiesterase inhibitor zaprinast. Inhibition of CDPK2A or CDPK1 caused a significant reduction in egress (**Fig. 1G–H**). By contrast, CDPK3 inhibition simply delayed egress ($T_{half\text{-}max}$ of 257 s versus 117 s for vehicle-treated parasites), with parasites eventually reaching levels of egress equivalent to $CDPK3^{M}$ (**Fig. 1G–H, Fig. S1D**). These differences were attributable to egress because similar numbers of vacuoles were present in all samples (**Fig. S1E**). The findings are consistent with previous work suggesting that PKG activation, through inhibition of the cGMP-degrading phosphodiesterases, can compensate for inhibition of CDPK3 (19, 54).

**The N-terminal extension of CDPK2A impacts its localization and function**

CDPK2A has a long N-terminal extension, which is absent from CDPK1 and CDPK3 (37). We examined whether the N-terminal extension is required for CDPK2A function. Attempts to amplify the 5′ end of *CDPK2A* from cDNA yielded two isoforms, which were used to clone two complementation constructs expressed under the heterologous *SAG1* promoter. Complement 1 (c.1) and complement 2 (c.2) differ in how much of the N-terminal extension they include due to alternative splicing; however, both constructs contain the entire kinase domain (**Fig. 2A**). We also generated complement 3 (c.3), which included 1.5 kb of sequence upstream of the predicted translational start site, as well as the first intron, enabling both isoforms to be expressed under endogenous regulation. Complementing alleles had Met

gatekeepers and C-terminal HA tags and were expressed in trans in CDPK2A$^{G}$ parasites (**Fig. 2A, Fig. S2A**). This strategy enables inhibition of the endogenous CDPK2A$^{G}$ to assess the functionality of the second copy. The selected clones ---exhibited comparable levels of CDPK2A$^{M}$ expression (**Fig. 2B**). We found that endogenously-tagged CDPK2A (Ty) localizes to the periphery of intracellular parasites, possibly to the inner membrane complex or PM (**Fig. 2C**). Out of the three complementing vectors, only c.3, which retained the endogenous 5′ end of the *CDPK2A* mRNA, localized to the parasite periphery, similarly to the endogenous copy. By contrast, c.1 and c.2 localized to the parasite cytosol (**Fig. 2C**). This suggested that localization to the parasite periphery is dependent on the endogenous 5′ end of the gene, though not necessarily the presence of the N-terminal extension, perhaps due to a cryptic alternative start site or the precise timing of expression.

We next assessed the function of the complementing alleles. We inhibited the endogenous CDPK2A$^{G}$ allele and assessed whether each of the complemented strains could egress following A23187 or zaprinast induction. With A23187 stimulation, c.1 and c.3 strains egressed normally despite inhibition of the endogenous allele; however, inhibitor-treated c.2 parasites exhibited no complementation (**Fig. 2D–E**). The two alleles that did complement (c.1 and c.3) had egress kinetics comparable to 3-MB-PP1–resistant CDPK2A$^{M}$ parasites, reaching half the maximal egress around 200 s (**Fig. S2B**). We confirmed that in all cases the monolayers were equivalently infected (**Fig. S2C**). Complementation during zaprinast-induced egress was intermediate but followed similar trends, with nearly-wild-type responses for c.3, an intermediate response for c.1, and no apparent complementation by c.2 (**Fig. 2F–G**). This partial rescue was also reflected in the rates of egress (**Fig. S2D–E**). These findings suggest that the N-terminal extension of CDPK2A—present in c.1 and c.3 constructs, but absent in c.2—is required for parasite egress. The functional complementation contrasts with the localization of the proteins encoded by these alleles, where only c.1 matched the peripheral localization of protein encoded by the endogenous allele.

**Conditional depletion of CDPK2A only partially mimics chemical inhibition**

Off-target effects of 3-MB-PP1 interfere with the chemical-genetic approach described above during long-term culture, making it challenging to assess the impact of kinase inhibition over several lytic cycles (56). Auxin-inducible degradation of target proteins has been adapted to *Toxoplasma* and used to investigate protein kinases and associated signaling pathways (57, 58). We employed this conditional-depletion system as an orthogonal strategy to assess CDPK function. Briefly, a protein of interest is tagged with an auxin-inducible degron (AID) in a strain expressing TIR1. When transgenic parasites are treated with the plant hormone auxin—most commonly 3-indoleacetic acid (IAA)—the tagged protein is ubiquitinated and targeted by the proteasome for degradation (59) (**Fig. 3A**). Protein depletion occurs within minutes to hours in *Toxoplasma*, depending on the protein of interest (57, 58). We generated a panel of strains in which CDPK1, CDPK3, or CDPK2A were tagged at their C termini with the Ty epitope followed by mNeonGreen and a minimal auxin-inducible degron (mAID; **Fig. S3A**). Localization of CDPK2A-AID was consistent with the chemical-genetic alleles, with mNeonGreen signal observed at the parasite periphery (**Fig. 3B**). Expression of all mNeonGreen-tagged alleles was measured by FACS in parasites with and without IAA treatment. Three hours of IAA treatment was sufficient to observe robust and uniform depletion of each CDPK (**Fig. 3C**). Based on these results, we treated the parasites

with auxin for a minimum of 3 h for downstream analyses, achieving kinase degradation within less than a single cell cycle.

We assessed egress following acute depletion of CDPK1, CDPK3, or CDPK2A. Stimulation with A23187 induced minimal egress in CDPK-depleted parasites, indicating that all three kinases are necessary for egress under these conditions (**Fig. 3D–E**); this is consistent with our chemical-genetic approach. Analysis of egress kinetics showed that all three depleted lines failed to egress within the observation window, in contrast to the TIR1 parental parasites, which achieved half-maximum egress in 115 s (**Fig. S3B–C**).

We next assessed the ability of CDPK-depleted parasites to egress in response to zaprinast stimulation. Depletion of CDPK1 or CDPK3 phenocopied their chemical-genetic inhibition. CDPK1-depleted parasites were unable to egress, whereas CDPK3-depleted parasites displayed delayed but near-complete egress (**Fig. 3F–G**), achieving half-maximum egress at 260 s compared to 120 s for the parental TIR1 strain (**Fig. S3D**). Surprisingly, CDPK2A-depleted parasites achieved normal levels of egress (90% of vehicle-treated parasites), albeit with a delay ($T_{half\text{-}max}$ of 230 s), despite equivalent levels of overall infection (**Fig. 3F–G, Fig S3D–E**). We conclude that differences between the strains used for chemical inhibition or depletion render CDPK2A differentially required for egress. Such differences may result from manipulation of the *CDPK2A* locus or the strain background in which the mutants were generated.

**Inhibition of CDPK1 reveals epistasis with CDPK2A**

We considered whether differences in the CDPK1 alleles of the parental lines used—$CDPK1^{M}$ for chemical genetics and $CDPK1^{G}$ for conditional depletion—could lead to the differential requirement for CDPK2A in zaprinast-stimulated egress when assessed by either approach. Enzymatic assays have demonstrated that $CDPK1^{G}$ is more catalytically active than $CDPK1^{M}$, although either allele can support parasite replication (60). Based on the presence of $CDPK1^{M}$ in the analogue-sensitive (AS) kinase lines and the observed overlapping phenotypes of CDPK1 and CDPK2A, we hypothesized that partial loss of CDPK1 activity may lead to an increased reliance on CDPK2A for egress.

We assessed whether CDPK1 and CDPK2A exhibit epistasis by broadly examining the lytic cycle during plaque formation. We partially inhibited CDPK1 with sublethal concentrations of 3-MB-PP1 in the context of CDPK2A expression or depletion, using the CDPK2A-AID strain. CDPK2A-depleted parasites failed to form plaques when CDPK1 was partially inhibited. By contrast, plaquing was not impacted by partial inhibition of CDPK1 in the context of CDPK3 depletion (**Fig. 4A**). This suggests that the requirement for CDPK2A during the lytic cycle depends on the level of CDPK1 activity.

We next examined the epistatic interaction between the two kinases during zaprinast-stimulated egress using endpoint assays. Treating parasites with a range of 3-MB-PP1 concentrations to inhibit $CDPK1^{G}$, we observed that CDPK2A depletion renders parasites hypersensitive to CDPK1 inhibition (**Fig. 4B, Fig. S4**). By contrast, depletion of CDPK3 did not change the sensitivity of parasites to CDPK1 inhibition by 3-MB-PP1; significance was calculated using an F test for fitting all data to a single curve—CDPK2A-AID data points did not fit a single curve ($p<0.0001$), whereas TIR1 and CDPK3-AID data points, irrespective of IAA treatment, fit to one curve (ns). This observation is supported by the calculated $EC_{50}$ for 3-MB-PP1, which decreases significantly when CDPK2A-AID parasites are treated

with auxin (**Fig. 4C**). The combination of chemical inhibition and protein knockdown allowed us to demonstrate that CDPK2A becomes more critical for egress when CDPK1 activity is compromised due to a mutant gatekeeper allele as in CDPK1$^{M}$ or chemical inhibition. We surmise that the AID-tagged lines more closely reflect physiological conditions—with a wildtype CDPK1 allele—than AS kinase lines, so we examined the function of CDPK2A across the lytic cycle using conditional depletion.

**Conditional depletion reveals a role for CDPK2A at various stages of the lytic cycle**

Plaque formation captures repeated cycles of host cell lysis. As expected, depletion of CDPK1 blocked plaque formation (47), whereas CDPK3 appeared completely dispensable (41, 49, 53). Depletion of CDPK2A resulted in the formation of fewer plaques than the vehicle-treated tagged line (**Fig. 5A, Fig. S5A**). These results are in line with the phenotype scores in the genome-wide fitness screen (49), placing CDPK2A at an intermediate fitness contribution, between CDPK1 and CDPK3. Additionally, CDPK2A-AID parasites formed smaller plaques than the parental line, and plaque size further decreased when CDPK2A was depleted by IAA treatment (**Fig. 5B, Fig. S5B**). The observed hypomorphism between CDPK2A-AID and parental TIR1 parasites suggests that AID-tagging of the kinase may impact its function. The impact of CDPK2A depletion on plaquing efficiency may result from impaired or inefficient invasion, slower parasite replication, decreased motility of parasites during successive rounds of lysis, or a combination thereof, which must be deconvoluted through single-phenotype assays.

We assessed whether CDPK2A is required for parasite invasion of host cells using an immunofluorescence assay that distinguishes between invaded and extracellular parasites. Depletion of CDPK1 blocked parasite invasion; however, depletion of CDPK3 or CDPK2A did not affect parasite invasion (**Fig. 5C**), consistent with previous findings for CDPK1 and CDPK3(19, 41, 47). The dispensability of CDPK2A for invasion was corroborated by chemical-genetics. Inhibition of analog-sensitive alleles of CDPK1 or CDPK2A with 3-MB-PP1 confirmed that CDPK1 is necessary for invasion, whereas CDPK2A is dispensable for this process (**Fig. S5C**).

Gliding motility precedes invasion and is a necessary aspect of parasite egress from host cells, making it critical for parasite spread (61). We quantitatively assessed the 3D motility of CDPK-depleted parasites in Matrigel, which may better capture subtle motility defects that are hard to appreciate by traditional 2D motility assessment (62) (**Fig. 5D**). Depletion of CDPK1 or CDPK3 decreased the percentage of parasites moving during the assay by 58% or 44% respectively. CDPK2A-AID parasites appeared to move less than the parental TIR1 strain, although their motility was not decreased further by pre-treatment with IAA (**Fig. 5E**). We directly compared the motility of TIR1 parental and CDPK2A-AID tagged parasites without the addition of IAA, confirming that CDPK2A-AID tagging decreased parasite motility significantly (**Fig. 5F**). Track length and displacement were significantly altered by addition of IAA to CDPK1-AID parasites only, and maximum and speed mean speed were not altered by IAA treatment in any of the strains analyzed (**Fig. S5D–G**). Consistent with our observations, CDPK1 was previously implicated in parasite motility in two-dimensional analyses (19, 47). There is some ambiguity as to CDPK3's contribution to parasite motility in previous 2D analyses, depending on whether parasites were stimulated by switching from intracellular to extracellular buffer (19, 53, 63) or by treatment with A23187(41). Nevertheless, it is clear that CDPK3-mediated phosphorylation of MyoA contributes to

motility (63). Our results suggest that CDPK2A, along with CDPK1 and CDPK3, plays a critical role in gliding motility; however, AID tagging seems to sufficiently reduce CDPK2A activity such that no further reduction in gliding motility is observed under IAA treatment. We expect that certain phenotypes might require higher levels of kinase activity, revealing the hypomorphism of the conditional allele.

We further assessed the ability of CDPK2A-depleted parasites to secrete micronemal contents. We expressed Gaussia luciferase (GLuc) fused to myc-tagged MIC2 in CDPK-AID transgenic lines in order to study microneme protein secretion following knockdown of each kinase (**Fig. S5H**). Following CDPK depletion, parasites were stimulated to secrete with fetal bovine serum (FBS) alone or supplemented with zaprinast. Excreted/secreted antigen (ESA)-containing supernatants were collected, and MIC2 secretion was measured by luciferase signal. Parasites depleted of CDPK1, CDPK3, or CDPK2A secreted less MIC2 when stimulated with either FBS alone or FBS and zaprinast for 30 min (**Fig. 5G**). Interestingly, CDPK2A is not required for zaprinast-stimulated microneme protein secretion at an acute 5 min time point, even though CDPK1 and CDPK3 are each required (**Fig. S5I**). We further verified that basal MIC2 levels were equivalent between strains and that CDPK depletion does not impact total MIC2 in parasite lysates (**Fig. S5J**). Overall, these results suggest CDPK1, CDPK3, and CDPK2A are all involved in microneme protein secretion, but to different degrees.

## DISCUSSION

We examined the role of CDPK2A in the lytic cycle of *Toxoplasma*, analyzing its contribution to parasite fitness through processes related to parasitism, including microneme protein secretion, gliding motility, and egress from host cells. Using a combination of chemical-genetic and conditional depletion methods, we show that CDPK2A contributes to the initiation of parasite egress through microneme discharge and gliding motility. We further demonstrated that the N-terminal extension of CDPK2A is necessary for the protein's function in egress. Contrasting results from chemical inhibition and conditional depletion studies revealed an epistatic interaction between CDPK2A and CDPK1. Our results suggest that CDPK2A and CDPK1 work together to mediate egress following the stimulation of the PKG pathway (**Fig. 5H**). This signaling module might be differentially compartmentalized from CDPK3 and PKG, which localize to the PM. Our work uncovered additional complexity and interconnectedness in the signaling pathways that govern key events during the parasite lytic cycle.

CDPK2A contributes to parasite fitness. Plaque assays showed limited growth for parasites depleted of CDPK2A—an intermediate effect between the dispensable CDPK3 and the essential CDPK1. These observations are consistent with previous genome-wide loss-of-function screens, which had calculated an intermediate phenotype for CDPK2A, between CDPK1 and CDPK3(49). We have sought to determine what differentiates the fitness-conferring CDPK1 and CDPK2A from the dispensable CDPK3. Chemical-genetic approaches previously showed that accumulation of cGMP, which activates PKG, can compensate for loss of CDPK3 during egress (19). The reliance on CDPK2A similarly appeared to be conditional on the activity of other kinases. While all three CDPKs were required for egress in response to calcium ionophores, as with CDPK3, conditional depletion of CDPK2A could be partially compensated through hyperstimulation of the PKG pathway; however, in the case of CDPK2A, compensation depended on the level of CDPK1 activity.

Epistasis appears pervasive among the pathways regulated by CDPKs. As mentioned above, activation of PKG through the application of phosphodiesterase inhibitors (e.g., zaprinast) enables parasite egress despite CDPK3 inhibition or loss (19, 54). Epistasis between PKG and CDPKs has also been observed in *Plasmodium* spp. at various stages of the intraerythrocytic cycle (15, 64, 65). Genetic interaction between PbCDPK4 (the ortholog of TgCDPK1) and PKG was revealed by a *P. berghei* screen (15). Analogously to our chemical-genetic results, PbCDPK4 becomes critical for parasite invasion and motility in a genetic background expressing a variant of PKG in which the gatekeeper residue has been mutated ($PKG^{T619Q}$) (15). It is inferred from phenotypes associated with PKG activity that the $PKG^{T619Q}$ mutant is less active than wildtype. As with the $TgCDPK1^{G128M}$ allele used in our chemical-genetic approach, these mutants retain sufficient kinase activity to sustain parasite viability, yet the mutation clearly places a strain on other aspects of the signaling network. Such interactions likely extend further into the network, since double knockouts of PbCDPK1 and PbCDPK4 are viable but cannot be generated in parasites expressing $PKG^{T619Q}$ (15). The interconnectivity of CDPK networks may render them more plastic. Indeed, studies in *P. falciparum* suggest that parasites rapidly adapt to the loss of PfCDPK1 activity, perhaps through upregulation of other CDPKs (65, 66).

The plasticity of the signaling networks controlling egress can be manipulated through pharmacological stimuli that obscure or exaggerate the function of individual pathway components, revealing novel connectivity or dependencies. As described above, hyperactivation of the PKG pathway overcomes inhibition of CDPK2A or CDPK3. Analogously, *P. falciparum* parasites deficient in CDPK5 fail to egress, but this block can be overcome by hyperactivation of PKG (10, 48)). The degree of pathway overstimulation, whether through ionophore or phosphodiesterase inhibitor treatment, influences the interpretation of the results—particularly since the natural levels or dynamics of these second messengers are rarely known. Hyperactivation of a pathway may also force interactions that would otherwise not occur at the basal state (67). With this context, we can consider that epistatic interactions may result from shared substrates or the redundancy of independent pathways. PKG has been shown to be a calcium regulator in *T. gondii* and *Plasmodium* spp.(7, 15–17, 68), placing it upstream of CDPK activation. In plants, CDPKs are tuned to respond to different calcium concentrations (38), raising the possibility that dependency on different parasite CDPKs may result from the magnitude of the calcium surge elicited by PKG. Nevertheless, the subcellular sorting of epistatic interactions—with CDPK3 and PKG strictly localized to the PM—argues for potential overlap in their substrates as the mechanism underlying their epistasis.

Our studies also reflect some of the challenges inherent in studying protein kinases and interconnected signaling networks. While the goal is often to infer the role of a kinase in its native state, genetic perturbations may result in compensatory changes that obscure its function. While AID knockdown of CDPK1 and CDPK3 phenocopied chemical-genetic findings for egress, CDPK2A knockdown did not. Surprisingly, the discrepancy between chemical inhibition and AID depletion of CDPK2A could be attributed to the difference in CDPK1 alleles between the two systems, since partial inhibition of CDPK1 results in a stronger requirement for CDPK2A in zaprinast-stimulated egress. This is consistent with biochemical studies that had revealed reduced ATP affinity of $TgCDPK1^{G128M}$ relative to the wildtype enzyme (60). Analogously, phenotypic assays such as 3D gliding motility and plaque size argue for hypomorphism of the CDPK2A-AID allele. Inspection of CDPK2A-AID parasites' motility tracks

suggested they may move along less-tightly-wound (or lower amplitude) corkscrews compared to other strains. An altered geometry of movement may be less efficient, resulting in the smaller plaque areas observed for CDPK2A-AID parasites. Taken together, these results argue for caution in the interpretation of perturbed signaling systems; nevertheless, comparison of multiple approaches can be used to infer the native function of protein kinases like CDPK2A.

Several signaling pathways converge on the regulation of microneme discharge, including those controlled by CDPK2A. Microneme discharge lies upstream of parasite egress, gliding motility, and invasion through the release of diverse proteins, including perforins that disrupt the PVM (29) and adhesins that mediate substrate attachment (69, 70). Depletion of any of the studied CDPKs resulted in a decrease in microneme discharge. The effect of CDPK2A depletion was only evident following prolonged periods of microneme discharge (30 min). By contrast, the effect of CDPK1 and CDPK3 was already evident within 5 min of stimulation. This may suggest a model in which some CDPKs regulate an initial wave of secretion, while others regulate the sustained response. Previous studies of CDPK3-knockout parasites reported normal MIC2 secretion for extracellular parasites stimulated with A23187 or ethanol (41), although intracellular parasites clearly depend on CDPK3 to permeabilize the parasitophorous vacuole upon A23187 treatment (19, 41). Differences in the sensitivity or conditions of our assays (e.g., the use of intracellular buffer in our microneme discharge assays) may have focused our assays on the responses that govern egress. Previous work also reported that the contributions of CDPK1 and CDPK3 to microneme discharge depended on the agonist used (19). Consistent with these observations and the epistatic interactions discussed above, CDPK2A may impact microneme secretion to different extents across the lytic cycle depending on the stimuli experienced by parasites.

We demonstrated that the N-terminal extension of CDPK2A is necessary for its function. Complementing constructs that expressed a full-length version of CDPK2A were able to egress when the endogenous kinase was inhibited. The N terminus may contain localization determinants that drive CDPK2A to the parasite periphery, although the predicted gene model lacks consensus motifs for myristoylation or palmitoylation that participate in the localization of CDPK3 to the PM (19, 41). CDPK2A was also not detected in mass spectrometry datasets enriching for myristoylated (71) or palmitoylated (72) proteins. Proteomic studies have detected CDPK2A peptides spanning the coding sequence of exon 2 (exon 1 in c.1), further suggesting that the truncated c.2 sequence generated from cDNA is not the prominent species in wild-type parasites (71). Only the complementing construct driven by the endogenous 5′ UTR and promoter yielded a protein that co-localized with the endogenous CDPK2A, suggesting localization to the parasite periphery depends on endogenous regulatory signals rather than the N terminus of the protein. We cannot exclude that an alternative translation start site is used, giving rise to dually-localized species. Methionine 59 in the longer gene model may be the true start site, matching the predicted coding sequence in *Hammondia hammondi* (73). The existing data suggest that localization to the parasite periphery is not strictly required for CDPK2A's function, in contrast to CDPK3, which must be peripherally-localized via myristoylation and palmitoylation in order for parasites to egress (19, 41). CDPK orthologs containing N-terminal extensions appear not to universally localize to any given compartment. PfCDPK5, which controls egress, associates with parasite membranes, possibly including the cytosolic-facing side of micronemes (10, 48), while PfCDPK3, required for ookinete motility, is cytoplasmic (11, 74). There is also precedent for signaling-

related proteins to express multiple functionally distinct isoforms, often arising from alternative translational initiation. For example, in *E. tenella* and *T. gondii*, one isoform of PKG is N-acylated and localizes to the PM, while the other isoform is cytoplasmic. Interestingly, either isoform can function if targeted to the PM (58, 75). Isoform diversity may further drive the plasticity of CDPK signaling networks, although this has not been formally addressed by our work.

The use of both chemical inhibition and conditional depletion to study CDPK2A function uncovered additional complexity and interconnectedness in the signaling pathways that govern the lytic cycle. We observe that CDPK1, CDPK3, and CDPK2A are all involved to varying degrees in microneme discharge, with functional consequences during egress, gliding motility, and invasion. We also further describe functional redundancy that structures the pathway into two signaling modules that are jointly required during parasite egress. CDPK1 and PKG play dominant roles in their respective modules, with CDPK2A and CDPK3 contributing less-essential functions. These supportive activities may be nonetheless important for parasite fitness under particular conditions. Additionally, these functional modules seem to be spatially distinct, with CDPK1/CDPK2A signaling occurring in the parasite cytoplasm, while CDPK3/PKG signaling occurs at the parasite PM (68). Understanding the topology of signaling pathways underlying key events in the parasite life cycle can help identify compensatory changes and predict phenotypic plasticity as we contemplate targeting parasite kinases for anti-parasitic therapies.

## MATERIALS & METHODS

### Parasite and host cell culture

*T. gondii* parasites were grown in human foreskin fibroblasts (HFFs) maintained in DMEM (GIBCO) supplemented with 3% heat-inactivated newborn calf serum (Millipore Sigma), 2mM L-glutamine (Thermo Fisher Scientific), and 10 µg/mL gentamicin (Thermo Fisher Scientific). Where noted, DMEM supplemented with 10% heat-inactivated fetal bovine serum (FBS, Millipore Sigma), 2mM L-glutamine (Thermo Fisher Scientific), and 10 µg/mL gentamicin was used. HFFs and *T. gondii* lines were monitored regularly and maintained as mycoplasma-free.

### Parasite transfection

Parasites were passed through 3 µm filters, pelleted at 1000 × *g* for 10 min, washed, resuspended in Cytomix (10 mM $KPO_4$, 120 mM KCl, 150 mM $CaCl_2$, 5 mM $MgCl_2$, 25 mM HEPES, 2 mM EDTA, 2 mM ATP, and 5 mM glutathione), and combined with DNA to a final volume of 400 µL. Electroporation used an ECM 830 Square Wave electroporator (BTX) in 4 mm cuvettes with the following settings: 1.7 kV, 2 pulses, 176 µs pulse length, and 100 ms interval.

### Strain generation

Oligos were ordered from IDT. Primers, plasmids, and parasite strains used or generated in this study can be found in **Supplementary Table 1**. Descriptions of strain generation and plasmid construction, or relevant accession numbers, are also provided in the table.

### cDNA generation

Total RNA was extracted from *RH* parasites using Trizol. cDNA was generated according to package instructions for SMARTer PCR cDNA synthesis kit (Clontech/TakaraBio).

### Genomic DNA extraction

Extracellular parasites were pelleted at 1000 × *g* for 10 min and resuspended in phosphate buffered saline supplemented with Proteinase K (10 µg/mL). Suspensions were incubated at 37□ for 1 h, 50□ for 2 h, 95□ for 15 min to extract genomic DNA.

**Immunoblotting**

Parasite pellets were lysed in xenopus buffer (50 mM KCl, 20 mM HEPES, 2 mM $MgCl_2$, 0.1 mM EDTA pH 7.5) supplemented with 1% TritonX-100, HALT protease inhibitor cocktail (ThermoFisher), and 10 µg/mL DNaseI (Sigma Aldrich) at room temperature for 1 hour with rotation. Lysates were combined with Laemmli buffer (for final concentration 2% SDS, 20% glycerol, 60 mM Tris HCl pH 6.8, 0.01% bromophenol blue) and 2-mercaptoethanol (1% final concentration) and boiled 10 min. Samples were run on a 7.5% SDS-PAGE gel (BioRad), transferred onto a nitrocellulose membrane in transfer buffer (25 mM TrisHCl, 192 mM glycine, 0.1% SDS, 20% methanol). Blocking and all subsequent antibody incubations were performed in 5% milk in TBS-T (20 mM Tris, 138 mM NaCl, 0.1% Tween-20). Primary and secondary antibody incubations proceeded for 1 h rocking at room temperature, with three TBS-T washes between primary and secondary and between secondary and imaging. Imaging was performed using a LI-COR Odyssey. Primary antibodies used were mouse anti-Ty (76) and rabbit anti-HA (71-5500, Invitrogen) or rabbit anti-TgACT1(77). Secondary antibodies were anti-mouse-800CW (LI-COR) or anti-rabbit-680RD (LI-COR).

**Live cell imaging**

Parasites were inoculated onto glass-bottom 35mm dishes (Mattek) containing HFFs. At 24 h post-infection, intracellular parasites were imaged with an Eclipse Ti microscope (Nikon) with a 60X objective using the NIS elements imaging software and a Zyla 4.2 sCMOS camera. FIJI software was used for image analysis and processing.

**Immunofluorescence assays**

Parasites were inoculated onto coverslips containing HFFs. At 24 h post-infection, intracellular parasites were fixed with 4% formaldehyde and permeabilized with 0.05% saponin in PBS. Nuclei were stained with Hoechst 33258 (Santa Cruz) and coverslips were mounted in Prolong Diamond (Thermo Fisher). Ty was detected using a mouse monoclonal antibody (76). HA was detected using a rabbit monoclonal antibody (71-5500, Invitrogen). Primary antibodies were detected with anti-mouse Alexa-Fluor 488 and anti-rabbit Alexa-Fluor 594 secondary antibodies (Invitrogen). Images were acquired with an Eclipse Ti microscope (Nikon) with a 60X objective using the NIS elements imaging software and a Zyla 4.2 sCMOS camera. FIJI software was used for image analysis and processing.

**Egress assays**

Egress was quantified in a plate-based manner as in (55). HFF monolayers in a clear bottomed 96-well plate were infected with parasites and allowed to incubate 24 h before exchanging media for FluoroBrite DMEM (ThermoFisher) supplemented with 10% FBS and applying pre-treatments according to experiment type. Three images were taken before zaprinast (final concentration 500 µM; MilliPore Sigma) or A23187 (final concentration 8 µM; MilliPore Sigma) and DAPI (final concentration 5□ ng□/mL) were added, and imaging of DAPI-stained host cell nuclei continued for 9 additional minutes before 1% Triton X-100 was added to all wells to determine the total number of host cell nuclei. Imaging was performed at 37°C and 5% $CO_2$ using a Biotek Cytation 3 imaging multimode reader with a 4X objective. % egress was calculated as [(nuclei at $time_n$ - nuclei at $time_1$)/(nuclei at $time_{final}$ – nuclei at $time_1$)] * 100, and egress efficiency was normalized to egress of vehicle-treated parasites (% vehicle). Results are the mean of three wells per condition and are representative of at least three independent

experiments. MOI was determined by performing immunofluorescence on a parallel plate of parasite-infected HFFs. Briefly, infected monolayers were fixed and permeabilized with 100% methanol for 2 min. Parasites were stained with either rabbit anti-TgALD (78) or guinea pig anti-CDPK1 antibody (79) and anti-rabbit or anti-guinea pig Alexa-Fluor 594 secondary antibody, and nuclei were stained with Hoechst 33258 (Santa Cruz Biotechnology). Imaging was performed using a Biotek Cytation 3 imaging multimode reader with a 20X objective, and parasite vacuoles and host nuclei were manually counted.

For AS kinase egress assays, HFFs were infected with $5 \times 10^4$ parasites per well and treated with 3 µM 3-MB-PP1 (MilliPore Sigma) or equivalent dilution of DMSO for 20 min prior to analysis.

For AID egress assays, HFFs were infected with $1 \times 10^5$ parasites per well of TIR1 parental or CDPK-AID lines and treated with 500 µM IAA or equivalent dilution of PBS for 3 h prior to analysis.

For epistasis endpoint assays, HFFs were infected with $1 \times 10^5$ parasites per well of TIR1 parental or CDPK-AID lines. Pre-treatment consisted of 500 µM IAA or equivalent dilution of PBS for 3 h, followed by 3-MB-PP1 (series from 2.5 µM to 0.039 µM) or equivalent dilution of DMSO for 30 min prior to analysis, and wells were stimulated to egress with zaprinast (final concentration 500 µM) for 20 min; all incubations were performed at 37°C and 5% $CO_2$. Images were collected pre-stimulation ($time_{pre}$), 10 min post addition of zaprinast (final concentration 500 µM) and DAPI ($time_{stim}$), and 1 min post addition of 1% TritonX-100 ($time_{final}$). % egress was calculated as [(nuclei at $time_{stim}$ - nuclei at $time_{pre}$)/(nuclei at $time_{final}$ – nuclei at $time_{pre}$)] * 100 and normalized to wells that did not receive IAA or 3-MB-PP1 for each strain. $EC_{50}$ was determined by non-linear regression analysis performed using the non-sigmoidal dose-response with variable slope function in GraphPad Prism, with top constrained to 100 and bottom constrained to 0; significance was calculated using an F test to determine if all data (±IAA) fit to a single curve.

**Invasion assays**

Briefly, parasite vacuoles were mechanically-dissociated and filtered through 5 µm filters, pelleted, and resuspended in invasion media (HEPES-buffered DMEM without phenol red) supplemented with 1% FBS. HFF monolayers in clear-bottom 96 well plates were incubated with parasite suspensions for 10 min at 37° to stimulate invasion after centrifuging the plates at 290 x *g* and room temperature for 5 min. Wells were fixed with 4% formaldehyde and followed by antibody staining to differentiate between extracellular and total parasites and to detect nuclei. Samples were imaged using a Biotek Cytation3 imaging multimode reader with a 20X objective and imaging in montage mode.

For AS kinase invasion assays, parasites were pre-treated with 3-MB-PP1 (0.33 µM final concentration) or an equivalent dilution of DMSO in invasion media for 20 min at 37°, then $1 \times 10^5$ parasites were added to 3 wells of a clear-bottom 96-well plate containing HFFs. Following incubation and fixation, extracellular parasites were stained with mouse anti-SAG1 antibody (80) conjugated to Alexa594. All parasites were stained by permeabilizing with 0.25% TritonX-100 and staining with anti-SAG1 antibody conjugated to Alexa488, and nuclei were stained with DAPI. The number of invaded parasites per field of view was counted using a size-based macro and normalized to the number of host cells in the same field of view (intracellular Tg/HCN). The final invasion efficiency for each replicate was normalized to the invaded parasites per host cell nuclei of the DMSO-treated parasites (% vehicle).

For AID invasion assays, parasite lines were each passed to two flasks of HFFs. 24 h pre-analysis one flask was supplemented with vehicle (PBS) and the second flask was supplemented with IAA to a final concentration of 500 µM. Following parasite harvest, $2 \times 10^5$ parasites were added to 3 wells of a clear-bottom 96-well plate containing HFFs. Following incubation and fixation, extracellular parasites were

stained with mouse anti-SAG1 antibody (80). All parasites were stained by permeabilizing with 0.25% TritonX-100 and staining with rabbit anti-GAP45, generated as previously described (81) and kindly provided by R.D. Ethridge (University of Georgia, Athens). Cells were subsequently stained with anti-rabbit Alexa594 antibody (Invitrogen), anti-mouse Alexa488 antibody (Invitrogen), and Hoechst 33258 (Santa Cruz Biotechnology). Images were acquired using a Cytation 3 imager (BioTek), and analyzed using custom FIJI macros to count the number of parasites and host-cell nuclei (49), plotted as intracellular Tg/HCN.

**Plaque assays**

CDPK-AID and TIR1 parental parasites were inoculated into 6-well plates or 15 cm dishes of HFFs maintained in DMEM supplemented with 10% FBS and incubated overnight before supplementing with IAA to a final concentration of 500 µM or with PBS. Where indicated, plates were also supplemented with 3-MB-PP1 to a final concentration of 40 nM or with DMSO. Plates were allowed to grow undisturbed for 8 days then washed with PBS and fixed for 10 min at room temperature with 100% ethanol. Staining was performed for 5 min at room temperature with crystal violet solution, followed by two washes with PBS, one wash with water, and drying overnight. Plaques were counted manually, and plaque areas measured using FIJI software.

**FACS analysis**

For IAA-induced depletion experiments, intracellular parasites were treated with either 500 µM IAA or an equivalent dilution of PBS for 1, 3, or 24 h. Following treatment, parasites were mechanically-dissociated by passing through a 27-gauge needle, isolated by filtration, and analyzed by flow cytometry with a Miltenyi MACSQuant VYB and plots were prepared using FlowJo software.

**Microneme protein secretion assays**

CDPK-GLuc lines were each used to inoculate two flasks of HFFs. 24 h pre-analysis one flask was supplemented with vehicle (PBS) and the second flask was supplemented with IAA to a final concentration of 500 µM. Parasite vacuoles were mechanically-disrupted and parasites filtered through 5 µm filters, pelleted, and resuspended in cold intracellular buffer with free $Ca^{2+}$ clamped at 100nM (ICB; 137mM KCl, 5mM NaCl, 20mM HEPES, 10mM $MgCl_2$). 1 x $10^6$ parasites were combined with ICB, ICB supplemented with 3% FBS, or ICB supplemented with zaprinast (500 µM) or an equivalent dilution of DMSO with or without 3% FBS into 3 wells of 96 well round-bottom plate and incubated for 5 or 30 min at 37□ to stimulate secretion. Excreted/secreted antigen (ESA)-containing supernatants were collected by centrifugation at 1200 x *g* for 8 min at 4□ to pellet parasites. Parasite lysates were prepared according to Pierce Gaussia Luciferase Glow Assay Kit (ThermoFisher) and plated in triplicate with wells containing lysate from 6.6 x $10^5$, 2.2 x $10^5$, and 7.4 x $10^4$ parasite-equivalents for each strain with or without IAA. ESAs and lysates were plated in white-bottom assay plates (PerkinElmer #6002290) and incubated at room temperature for 5 min with substrate-containing assay solution before detecting luciferase signal using a Biotek Cytation3 multimode reader. For each independent replicate, background luminescence (from wells without parasites) was subtracted from ESA luciferase values.

**3D Motility**

Parasites in HFF cells were treated with either 500 µM auxin or PBS for three hours prior to harvest by mechanical dissociation. Pitta imaging chambers containing Hoechst 33342-stained parasites embedded in polymerized Matrigel were prepared as previously described (62). A Nikon Eclipse TE300

609 epifluorescence microscope (Nikon Instruments, Melville, NY) equipped with a 20× (0.65 pixel/µm)
610 PlanApo λ (NA 0.75) objective and NanoScanZ piezo Z stage insert (Prior Scientific, Rockland, MA) was
611 used to image the fluorescently-labeled parasite nuclei. Time-lapse video stacks were collected with an
612 iXON Life 888 EMCCD camera (Andor Technology, Belfast, Ireland) using NIS Elements software v.5.11
613 (Nikon Instruments, Melville, NY) and pE-4000 LED illumination (CoolLED, Andover England). Images
614 (1024 pixel × 384 pixel) were collected 1 µm apart in *z*, spanning 40 µm. Each *z* slice was imaged twice,
615 at excitation wavelengths 385 nm (Hoechst) then 490 nm (mNeonGreen), each for 15 ms, before
616 moving to the next *z* slice. The same volume was successively imaged 60 times at both wavelengths
617 over the course of 78 seconds. The volume of each video stack was therefore 665.6 µm × 249.6 µm × 40
618 µm (*x, y, z*), and each dataset contained 2 x 60 stacks. The camera was set to trigger mode, no binning,
619 readout speed of 30 MHz, conversion gain of 3.8x, and EM gain setting of 300.

620 Datasets were analyzed in Imaris ×64 v. 9.2.0 (Bitplane AG, Zurich, Switzerland). Parasites were tracked
621 using the ImarisTrack module within a 1018 pixel × 380 pixel region of interest to prevent artifacts from
622 tracking objects near the border. Spot detection used estimated spot diameters of 4.0 × 4.0 × 8.0 µm (*x,*
623 *y, z)* for the fluorescently-labeled nuclei. A maximum distance of 6.0 µm and maximum gap size of 2
624 were applied to the tracking algorithm. Tracks with durations under ten seconds or displacements of
625 less than 2 µm were discarded to avoid tracking artifacts and parasites moving by Brownian motion,
626 respectively (62). Accurate tracking was confirmed by visual inspection of parasite movements
627 superimposed on their calculated trajectories. The mNeonGreen signal was used to confirm the
628 expected level of the mNeonGreen-Ty-AID-tagged CDPK protein in tracked parasites; parasites that
629 were treated with auxin and remained positive for mNeonGreen were excluded from the analysis. Each
630 experiment analyzed three biological replicates, each consisting of three technical replicates.

631 **Data Availability**

632 Primers, plasmids, and parasite strains used or generated in this study can be found in **Supplementary**
633 **Table 1**. Oligos, plasmids, and strains generated within this study are available from the corresponding
634 author by request.

635

636 ## ACKNOWLEDGEMENTS

637 We thank the L.D. Sibley (Washington University in St. Louis) for the TIR1 strain; S.M. Sidik for
638 generation of the Cas9 nickase plasmid; B.M. Markus for generation of the mNeonGreen-mAID-Ty
639 plasmid; R.D. Etheridge (University of Georgia, Athens) for the GAP45 antibody; VEuPathDB and all
640 contributors to this resource. This work was supported by grants from the National Institutes of Health
641 to S.L. (R01AI144369) and G.E.W. (R01AI139201), and training grant and fellowship support for R.V.S.
642 (T32AI055402 and F31AI145214).

643

644 ## AUTHOR CONTRIBUTIONS

645 E.S. and S.L. designed the overall study and experiments. C.G.H. generated and validated the AS-
646 kinase strains and performed initial construction of complementing constructs. R.V.S. performed and
647 quantified the gliding motility experiments. E.S. performed all remaining parasite strain construction

and experiments. E.S. and S.L. wrote the manuscript and all authors reviewed, offered input, and approved the final draft.

## FIGURES & LEGENDS

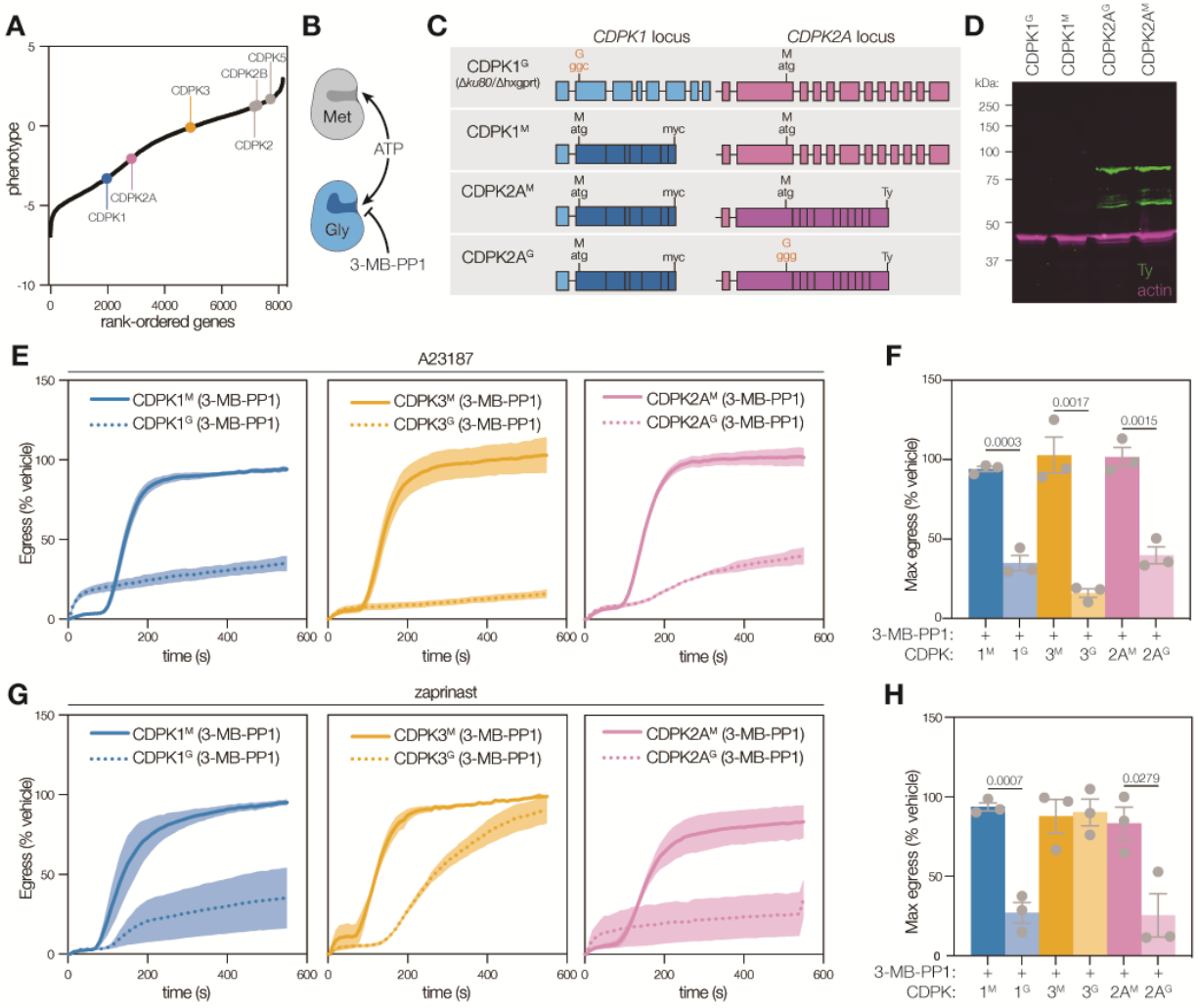


**Figure 1. CDPK2A is required for stimulated parasite egress in addition to CDPK1 and CDPK3. A.** *Toxoplasma* genes ranked by their phenotype, as determined in a genome-wide knockout screen (49). Points represent the mean phenotype score of $n = 4$ replicates. Six canonical calcium-dependent protein kinases are highlighted: CDPK1 (blue), CDPK3 (yellow), and CDPK2A (pink). **B.** Schematic representation of chemical-genetics strategy. The gatekeeper residue of a kinase of interest is mutated, with minimal impact to ATP binding but altered binding of bulky ATP-mimetic inhibitors (e.g., 3-MB-PP1) depending on the size of the binding pocket. **C.** Schematic representation of CDPK1 and CDPK2A loci in the analog-sensitive (AS) kinase strains. Darker shading indicates synthetic DNA. 3-MB-PP1–sensitive alleles are highlighted in red. **D.** Immunoblot of wildtype ($CDPK1^{G}$), parental ($CDPK1^{M}$), and Ty-tagged CDPK2A AS-kinase strains shows expression of the tagged kinase; ACT1 is used as a loading control. **E.** Kinetic traces of A23187-stimulated parasite egress. Graphs are egress of 3-MB-PP1–treated parasites as % of vehicle. A23187 was added 1 s after the start of imaging. Line plots represent the mean ± SEM for $n = 3$ biological replicates. **F.** Maximum egress achieved by each strain during the 10-minute observation window, displayed as % of vehicle. Bars represent the mean ± SEM of $n = 3$

667 biological replicates; significance calculated by unpaired *t*-test. **G.** Kinetic traces of zaprinast-stimulated
668 parasite egress. Graphs are egress of 3-MB-PP1–treated parasites as % of vehicle. Zaprinast was added
669 1 s after the start of imaging. Line plots the mean ± SEM for $n = 3$ biological replicates. **H.** Maximum
670 egress achieved by each strain during the 10-minute observation window, displayed as % of vehicle.
671 Bars represent the mean ± SEM of $n = 3$ biological replicates; significance calculated by unpaired *t*-test.
672

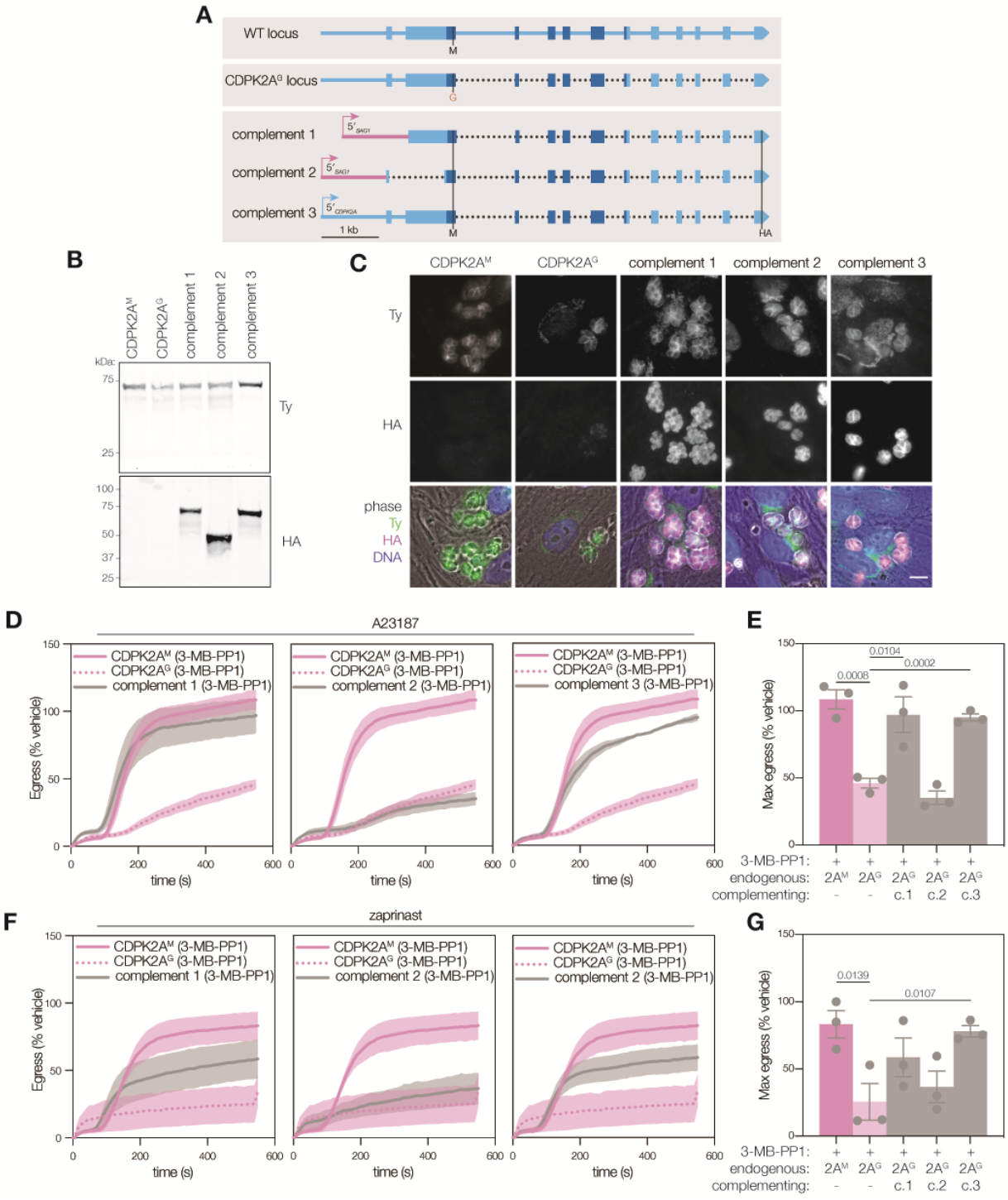


**Figure 2. The N-terminal extension of CDPK2A influences its localization and is necessary for parasite egress. A.** Schematic representation of complementing constructs with comparison to CDPK2A genomic locus. Dotted lines indicate gaps in sequence where introns have been removed. Shaded region encoding the kinase domain. **B.** Immunoblot of complemented strains probing for the endogenous allele with Ty and the complementing allele with HA. **C.** Immunofluorescence microscopy of endogenously Ty-tagged CDPK2A$^{M}$ and CDPK2A$^{G}$ and HA-tagged complementing copies of

CDPK2A$^{M}$. Merged image displays Ty (green), HA (magenta), DNA (blue), and phase (greyscale). Scale bar is 10 µm. **D.** Kinetic traces of A23187-stimulated parasite egress. Graphs are egress of 3-MB-PP1–treated parasites as % of vehicle. A23187 was added 1 s after the start of imaging. Line plots represent mean ± SEM for *n* = 3 biological replicates. **E.** Maximum egress achieved by each strain during the observation window, displayed as % of vehicle. Bars represent mean ± SEM of *n* = 3 biological replicates; significance calculated by unpaired one-tailed *t*-test. **F.** Kinetic traces of zaprinast-stimulated parasite egress. Graphs are egress of 3-MB-PP1–treated parasites as % of vehicle. Zaprinast was added 1 s after the start of imaging. Line plots represent mean ± SEM for *n* = 3 biological replicates. **G.** Maximum egress achieved by each strain during the observation window, displayed as % of vehicle. Bars represent the mean ± SEM of *n* = 3 biological replicates; significance calculated by unpaired one-tailed *t*-test.

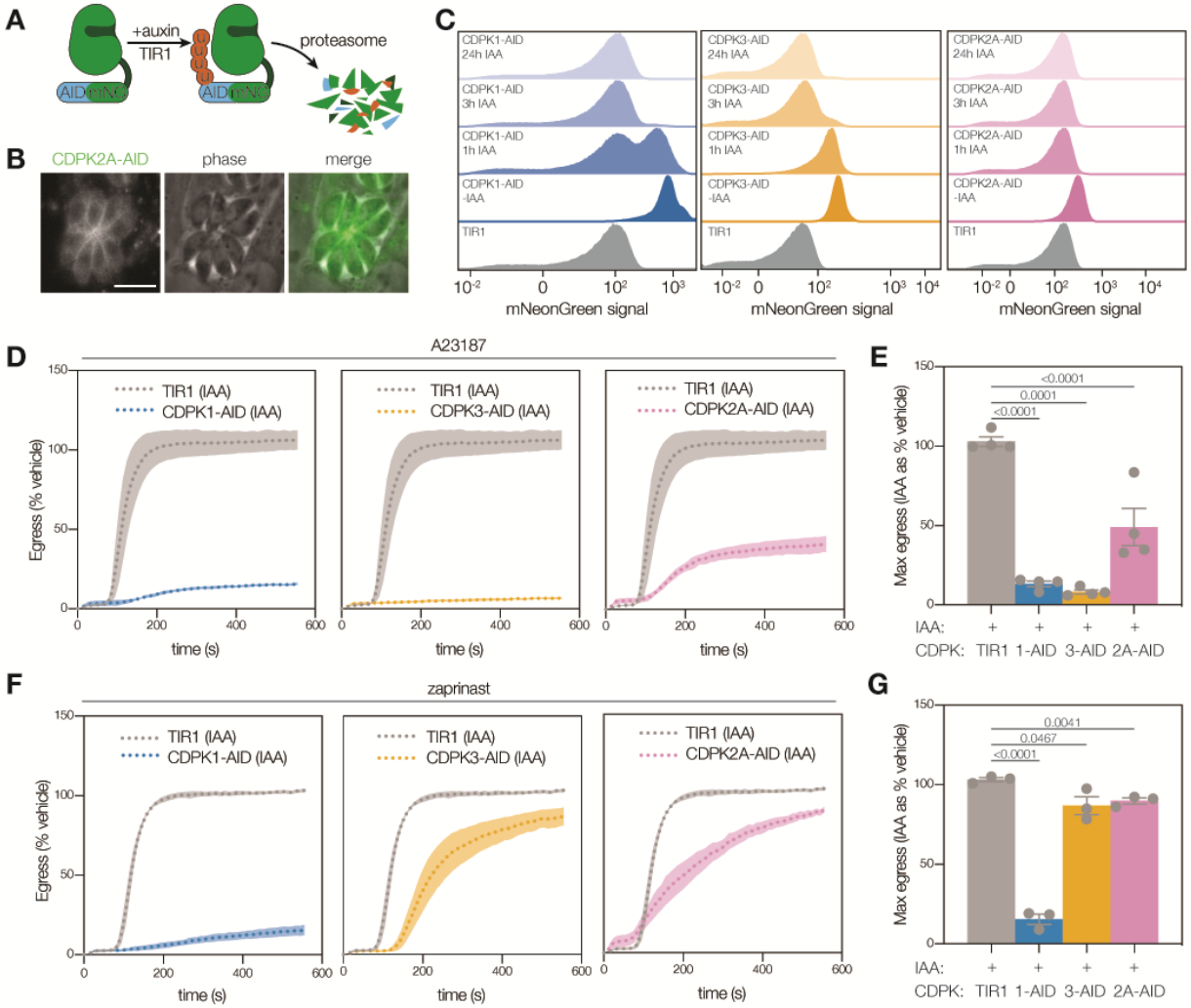


692

693 **Figure 3. Conditional depletion of CDPKs reveals CDPK2A is required for A23187-stimulated egress,**
694 **but not for zaprinast-stimulated egress. A.** Schematic representation of a CDPK tagged with a
695 minimal auxin-inducible degron (mAID), Ty, and mNeonGreen. When IAA is added, the TIR1 ubiquitin
696 ligase complex is recruited to the tagged protein and targets it for proteasomal degradation. **B.** Live-
697 cell imaging of CDPK2A-AID parasites shows the mNeonGreen signal concentrated at the parasite
698 periphery. Scale bar is 10 µm. **C.** FACS analysis of mNeonGreen-tagged CDPK-AID parasites and TIR1
699 parental line with and without the addition of auxin (IAA) shows expression of mNeonGreen fusion and
700 kinetics of auxin-induced depletion. **D.** Kinetic traces of A23187-stimulated parasite egress. Graphs are
701 egress of 3-MB-PP1–treated parasites as % of vehicle. A23187 was added 1 s after the start of imaging.
702 Line plots represent mean ± SEM for $n = 4$ biological replicates. **E.** Maximum egress achieved by each
703 strain during the observation window, displayed as % of vehicle. Bars represent mean ± SEM of $n = 4$
704 biological replicates; significance calculated by unpaired *t*-test. **F.** Kinetic traces of zaprinast-stimulated
705 parasite egress. Graphs are egress of 3-MB-PP1–treated parasites as % of vehicle. Zaprinast was added
706 1 s after the start of imaging. Line plots the mean for $n = 3$ biological replicates with error bands
707 representing SEM. **G.** Maximum egress achieved by each strain during the observation window,

displayed as % of vehicle. Bars represent the mean ± SEM of $n = 3$ biological replicates; significance calculated by unpaired *t*-test.

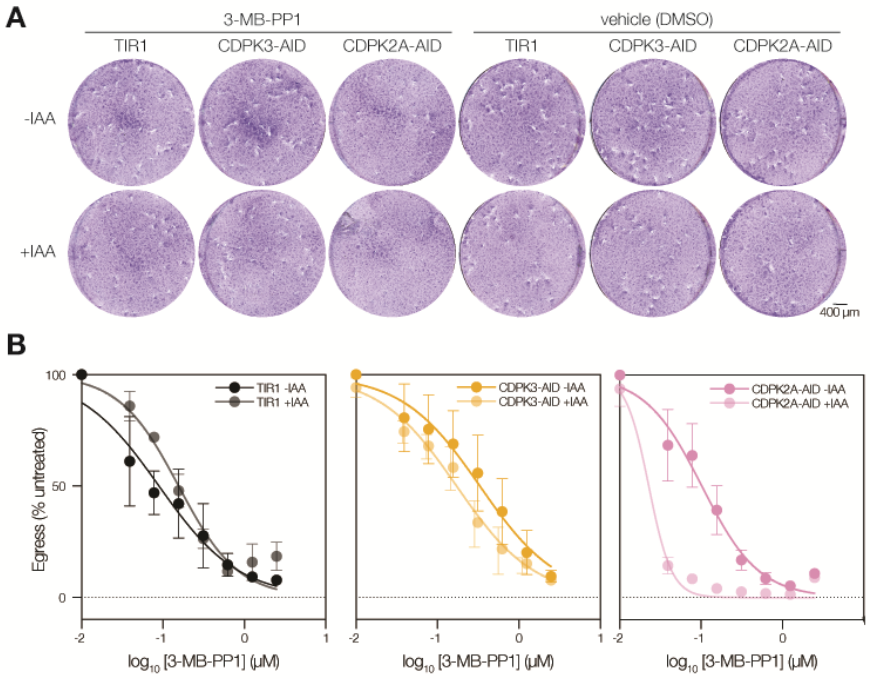


C

| | -IAA $EC_{50}$ (µM) (mean ± SEM) | +IAA $EC_{50}$ (µM) (mean ± SEM) | *p*-value |
|---|---|---|---|
| TIR1 | 0.12 ± 0.049 | 0.16 ± 0.018 | 0.2541 |
| CDPK3-AID | 0.46 ± 0.25 | 0.21 ± 0.084 | 0.1954 |
| CDPK2A-AID | 0.12 ± 0.039 | 0.023 ± 0.0034 | 0.0370 |

**Figure 4. CDPK1 and CDPK2A comprise a signaling module that regulates zaprinast-stimulated egress and the lytic cycle. A.** Partial inhibition of endogenous $CDPK1^G$ by 3-MB-PP1 (40nM) leads to ablation of plaque formation by parasites conditionally depleted of CDPK2A. Scale bar represents 400 µm. **B.** Dose-response of CDPK1 inhibition with 3-MB-PP1 monitoring endpoint zaprinast-stimulated egress in parasites depleted of or expressing the indicated CDPK. Mean ± SEM plotted for $n = 3$ biological replicates. **C.** $EC_{50}$ (µM) for 3-MB-PP1 of CDPK-depleted or untreated parasites; significance calculated by unpaired one-tailed *t*-test across $n = 3$ biological replicates.

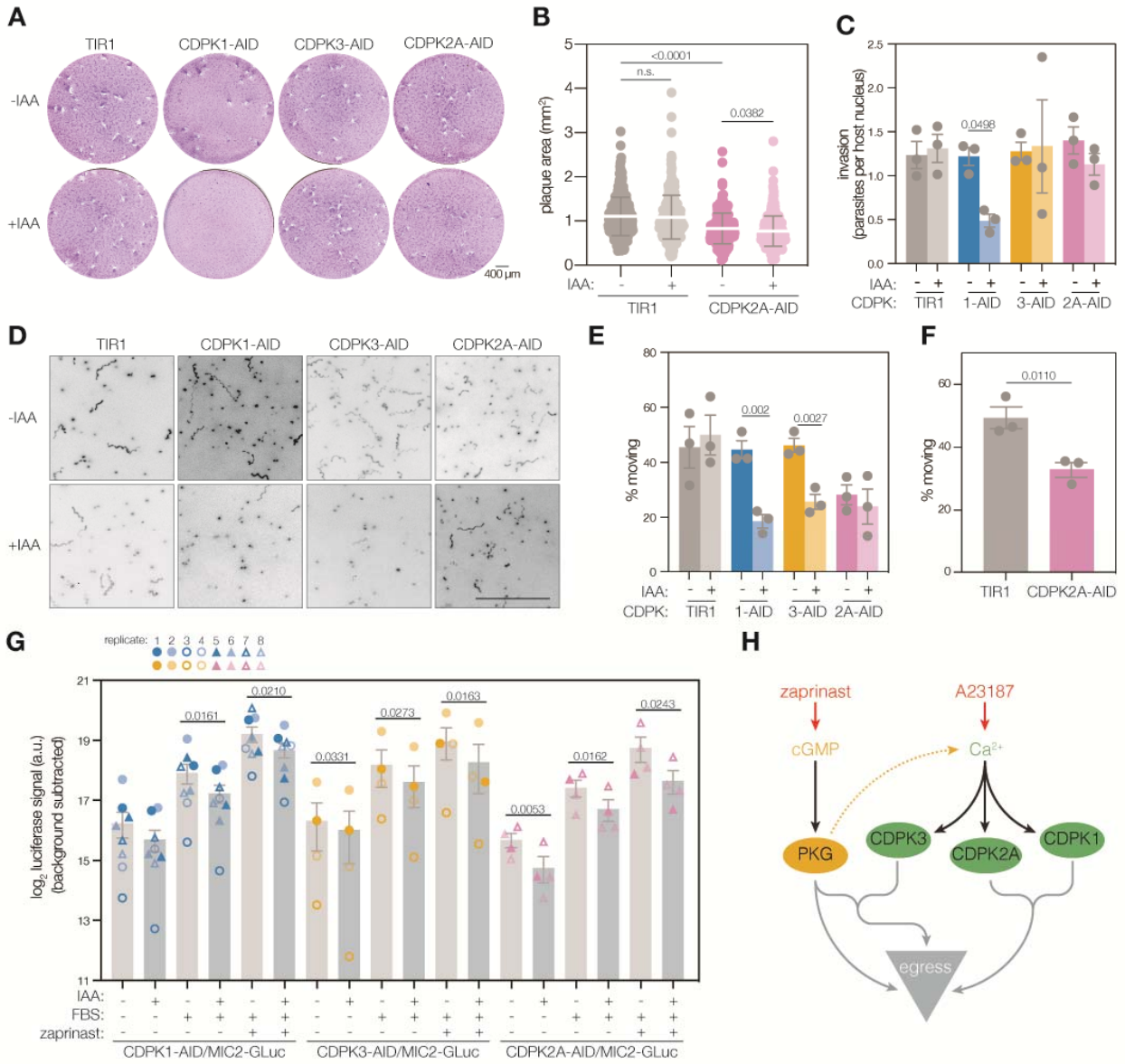


**Figure 5. CDPK2A impacts plaque formation, gliding motility, and microneme discharge. A.** Depletion of each of the three CDPKs impacted plaque formation differently: parasites depleted of CDPK1 formed no plaques, those depleted of CDPK2A formed smaller plaques, and those depleted of CDPK3 plaqued normally. Images are representative of $n = 4$ biological replicates. Scale bar is 400 µm. **B.** CDPK2A-AID parasites form smaller plaques than the TIR1 parental line, and the effect is exacerbated by the depletion of the kinase (+ IAA). Scatter plot displays areas for >270 individual plaques per sample; mean ± SD is overlaid; *p* value calculated by unpaired *t*-test. **C.** CDPK2A depletion does not impact parasites' ability to invade host cells. Bars represent the mean ± SEM for $n = 3$ biological replicates; *p* value calculated by paired *t*-test. **D.** 3D gliding motility in Matrigel following depletion of each kinase. Maximum intensity projections of tracked parasites. Scale bar is 100 µm. **E.** Proportion of parasites observed moving in 3D gliding motility assays. Each point is the mean of 3 technical replicates with 634-1500 observations per condition; bars represent the mean ± SEM of $n = 3$

biological replicates; significance calculated by unpaired one-tailed *t*-test. **F.** Direct comparison of the proportion of parasites gliding in 3D for TIR1 and CDPK2A-AID parasites without IAA. Each point is the mean of 3 technical replicates with 1011 and 1157 observations for TIR1 and CDPK2A-AID respectively; bars represent the mean ± SEM of $n = 3$ biological replicates; significance calculated by unpaired one-tailed *t*-test. **G.** Depletion of CDPKs decreases microneme discharge. Gaussia-luciferase activity, from a microneme-localized construct, was assayed in supernatants following 30 minutes of stimulation with FBS and zaprinast. Points represent individual biological replicates ($n = 8$ for CDPK1-AID, $n = 4$ for CDPK3-AID or CDPK2A-AID), with bars indicating mean ± SEM; significance calculated by paired one-tailed *t*-test. **H.** Proposed model for the relationship between kinases that positively regulate parasite motility.

## REFERENCES


1. Clapham DE. 2007. Calcium signaling. Cell 131:1047–1058.

2. Endo T, Sethi KK, Piekarski G. 1982. Toxoplasma gondii: calcium ionophore A23187-mediated exit of trophozoites from infected murine macrophages. Exp Parasitol 53:179–188.

3. Moreno SNJ, Zhong L. 1996. Acidocalcisomes in *Toxoplasma gondii* tachyzoites. Biochemical Journal https://doi.org/10.1042/bj3130655.

4. Stommel EW, Ely KH, Schwartzman JD, Kasper LH. 1997. Toxoplasma gondii: dithiol-induced Ca2+ flux causes egress of parasites from the parasitophorous vacuole. Exp Parasitol 87:88–97.

5. Borges-Pereira L, Budu A, McKnight CA, Moore CA, Vella SA, Hortua Triana MA, Liu J, Garcia CRS, Pace DA, Moreno SNJ. 2015. Calcium Signaling throughout the Toxoplasma gondii Lytic Cycle. J Biol Chem 290:26914–26926.

6. Lovett JL, Sibley LD. 2003. Intracellular calcium stores in Toxoplasma gondii govern invasion of host cells. J Cell Sci 116:3009–3016.

7. Sidik SM, Hortua Triana MA, Paul AS, El Bakkouri M, Hackett CG, Tran F, Westwood NJ, Hui R, Zuercher WJ, Duraisingh MT, Moreno SNJ, Lourido S. 2016. Using a Genetically Encoded Sensor to Identify Inhibitors of Toxoplasma gondii Ca2+ Signaling. J Biol Chem 291:9566–9580.

8. Singh S, Mahmood Alam M, Pal-Bhowmick I, Brzostowski JA, Chitnis CE. 2010. Distinct External Signals Trigger Sequential Release of Apical Organelles during Erythrocyte Invasion by Malaria Parasites. PLoS Pathogens https://doi.org/10.1371/journal.ppat.1000746.

9. Agarwal S, Singh MK, Garg S, Chitnis CE, Singh S. 2013. Ca(2+) -mediated exocytosis of subtilisin-like protease 1: a key step in egress of Plasmodium falciparum merozoites. Cell Microbiol 15:910–921.

10. Dvorin JD, Martyn DC, Patel SD, Grimley JS, Collins CR, Hopp CS, Bright AT, Westenberger S, Winzeler E, Blackman MJ, Baker DA, Wandless TJ, Duraisingh MT. 2010. A plant-like kinase in Plasmodium falciparum regulates parasite egress from erythrocytes. Science 328:910–912.

11. Siden-Kiamos I, Ecker A, Nyback S, Louis C, Sinden RE, Billker O. 2006. Plasmodium berghei calcium-dependent protein kinase 3 is required for ookinete gliding motility and mosquito midgut invasion. Molecular Microbiology https://doi.org/10.1111/j.1365-2958.2006.05189.x.

12. Wetzel DM, Chen LA, Ruiz FA, Moreno SNJ, Sibley LD. 2004. Calcium-mediated protein secretion potentiates motility in Toxoplasma gondii. J Cell Sci 117:5739–5748.

13. Pace DA, McKnight CA, Liu J, Jimenez V, Moreno SNJ. 2014. Calcium Entry in Toxoplasma gondiiand Its Enhancing Effect of Invasion-linked Traits. J Biol Chem 289:19637–19647.

776 14. Lourido S, Moreno SNJ. 2015. The calcium signaling toolkit of the Apicomplexan parasites
777 Toxoplasma gondii and Plasmodium spp. Cell Calcium 57:186–193.

778 15. Fang H, Gomes AR, Klages N, Pino P, Maco B, Walker EM, Zenonos ZA, Angrisano F, Baum J,
779 Doerig C, Baker DA, Billker O, Brochet M. 2018. Epistasis studies reveal redundancy among
780 calcium-dependent protein kinases in motility and invasion of malaria parasites. Nat Commun 9:1–
781 14.

782 16. Brown KM, Lourido S, Sibley LD. 2016. Serum Albumin Stimulates Protein Kinase G-dependent
783 Microneme Secretion in Toxoplasma gondii. J Biol Chem 291:9554–9565.

784 17. Brochet M, Collins MO, Smith TK, Thompson E, Sebastian S, Volkmann K, Schwach F, Chappell L,
785 Gomes AR, Berriman M, Rayner JC, Baker DA, Choudhary J, Billker O. 2014. Phosphoinositide
786 Metabolism Links cGMP-Dependent Protein Kinase G to Essential Ca2+ Signals at Key Decision
787 Points in the Life Cycle of Malaria Parasites 12:e1001806–15.

788 18. Howard BL, Harvey KL, Stewart RJ, Azevedo MF, Crabb BS, Jennings IG, Sanders PR, Manallack
789 DT, Thompson PE, Tonkin CJ, Gilson PR. 2015. Identification of potent phosphodiesterase
790 inhibitors that demonstrate cyclic nucleotide-dependent functions in apicomplexan parasites. ACS
791 Chem Biol 10:1145–1154.

792 19. Lourido S, Tang K, Sibley LD. 2012. Distinct signalling pathways control Toxoplasma egress and
793 host-cell invasion. EMBO J 31:4524–4534.

794 20. Collins CR, Hackett F, Strath M, Penzo M, Withers-Martinez C, Baker DA, Blackman MJ. 2013.
795 Malaria parasite cGMP-dependent protein kinase regulates blood stage merozoite secretory
796 organelle discharge and egress. PLoS Pathog 9:e1003344.

797 21. Bullen HE, Jia Y, Yamaryo-Botte Y, Bisio H, Zhang O, Jemelin NK, Marq J-B, Carruthers V, Botte
798 CY, Soldati-Favre D. 2016. Phosphatidic Acid-Mediated Signaling Regulates Microneme Secretion
799 in Toxoplasma. Cell Host Microbe 19:349–360.

800 22. Carruthers VB, Giddings OK, Sibley LD. 1999. Secretion of micronemal proteins is associated with
801 toxoplasma invasion of host cells. Cell Microbiol 1:225–235.

802 23. Carruthers VB, Sibley LD. 1999. Mobilization of intracellular calcium stimulates microneme
803 discharge in Toxoplasma gondii. Mol Microbiol 31:421–428.

804 24. Carruthers VB, Sherman GD, Sibley LD. 2000. The Toxoplasma adhesive protein MIC2 is
805 proteolytically processed at multiple sites by two parasite-derived proteases. J Biol Chem
806 275:14346–14353.

807 25. Jacot D, Tosetti N, Pires I, Stock J, Graindorge A, Hung Y-F, Han H, Tewari R, Kursula I, Soldati-
808 Favre D. 2016. An Apicomplexan Actin-Binding Protein Serves as a Connector and Lipid Sensor to
809 Coordinate Motility and Invasion. Cell Host Microbe 20:731–743.

26. Sultan AA, Thathy V, Frevert U, Robson KJ, Crisanti A, Nussenzweig V, Nussenzweig RS, Ménard R. 1997. TRAP is necessary for gliding motility and infectivity of plasmodium sporozoites. Cell 90:511–522.

27. Lagal V, Binder EM, Huynh M-H, Kafsack BFC, Harris PK, Diez R, Chen D, Cole RN, Carruthers VB, Kim K. 2010. Toxoplasma gondii protease TgSUB1 is required for cell surface processing of micronemal adhesive complexes and efficient adhesion of tachyzoites. Cell Microbiol 12:1792–1808.

28. Dowse T, Soldati D. 2004. Host cell invasion by the apicomplexans: the significance of microneme protein proteolysis. Curr Opin Microbiol 7:388–396.

29. Kafsack BFC, Pena JDO, Coppens I, Ravindran S, Boothroyd JC, Carruthers VB. 2009. Rapid membrane disruption by a perforin-like protein facilitates parasite exit from host cells. Science 323:530–533.

30. Sivagurunathan S, Heaslip A, Liu J, Hu K. 2013. Identification of functional modules of AKMT, a novel lysine methyltransferase regulating the motility of Toxoplasma gondii. Mol Biochem Parasitol 189:43–53.

31. Deligianni E, Morgan RN, Bertuccini L, Wirth CC, Silmon de Monerri NC, Spanos L, Blackman MJ, Louis C, Pradel G, Siden-Kiamos I. 2013. A perforin-like protein mediates disruption of the erythrocyte membrane during egress of Plasmodium berghei male gametocytes. Cell Microbiol 15:1438–1455.

32. Wirth CC, Glushakova S, Scheuermayer M, Repnik U, Garg S, Schaack D, Kachman MM, Weißbach T, Zimmerberg J, Dandekar T, Griffiths G, Chitnis CE, Singh S, Fischer R, Pradel G. 2014. Perforin-like protein PPLP 2 permeabilizes the red blood cell membrane during egress of *P lasmodium falciparum* gametocytes. Cellular Microbiology https://doi.org/10.1111/cmi.12288.

33. Garg S, Agarwal S, Kumar S, Yazdani SS, Chitnis CE, Singh S. 1AD. Calcium-dependent permeabilization of erythrocytes by a perforin-like protein during egress of malaria parasites. Nat Commun 4:1736–1712.

34. Chen X-M, O'Hara SP, Huang BQ, Nelson JB, Lin JJ-C, Zhu G, Ward HD, LaRusso NF. 2004. Apical Organelle Discharge by *Cryptosporidium parvum* Is Temperature, Cytoskeleton, and Intracellular Calcium Dependent and Required for Host Cell Invasion. Infection and Immunity https://doi.org/10.1128/iai.72.12.6806-6816.2004.

35. Wiersma HI, Galuska SE, Tomley FM, Sibley LD, Liberator PA, Donald RGK. 2004. A role for coccidian cGMP-dependent protein kinase in motility and invasion. Int J Parasitol 34:369–380.

36. Gantt S, Persson C, Rose K, Birkett AJ, Abagyan R, Nussenzweig V. 2000. Antibodies against thrombospondin-related anonymous protein do not inhibit Plasmodium sporozoite infectivity in

844 vivo. Infect Immun 68:3667–3673.

845 37. Billker O, Lourido S, Sibley LD. 2009. Calcium-dependent signaling and kinases in apicomplexan
846 parasites. Cell Host Microbe 5:612–622.

847 38. Harper JF, Breton G, Harmon A. 2004. DECODING $Ca^{2}$ SIGNALS THROUGH PLANT PROTEIN
848 KINASES. Annual Review of Plant Biology
849 https://doi.org/10.1146/annurev.arplant.55.031903.141627.

850 39. Harmon AC, Gribskov M, Harper JF. 2000. CDPKs - a kinase for every Ca2+ signal? Trends Plant Sci
851 5:154–159.

852 40. Lee JY, Yoo BC, Harmon AC. 1998. Kinetic and calcium-binding properties of three calcium-
853 dependent protein kinase isoenzymes from soybean. Biochemistry 37:6801–6809.

854 41. McCoy JM, Whitehead L, van Dooren GG, Tonkin CJ. 2012. TgCDPK3 regulates calcium-dependent
855 egress of Toxoplasma gondii from host cells. PLoS Pathog 8:e1003066.

856 42. Long S, Wang Q, Sibley LD. 2016. Analysis of Noncanonical Calcium-Dependent Protein Kinases in
857 Toxoplasma gondii by Targeted Gene Deletion Using CRISPR/Cas9. Infect Immun 84:1262–1273.

858 43. Morlon-Guyot J, Berry L, Chen C-T, Gubbels M-J, Lebrun M, Daher W. 2014. The Toxoplasma
859 gondii calcium-dependent protein kinase 7 is involved in early steps of parasite division and is
860 crucial for parasite survival. Cell Microbiol 16:95–114.

861 44. Bansal P, Antil N, Kumar M, Yamaryo-Botté Y, Rawat RS, Pinto S, Datta KK, Katris NJ, Botté CY,
862 Prasad TSK, Sharma P. 2021. Protein kinase TgCDPK7 regulates vesicular trafficking and
863 phospholipid synthesis in Toxoplasma gondii. PLoS Pathog 17:e1009325.

864 45. Billker O, Dechamps S, Tewari R, Wenig G, Franke-Fayard B, Brinkmann V. 2004. Calcium and a
865 calcium-dependent protein kinase regulate gamete formation and mosquito transmission in a
866 malaria parasite. Cell 117:503–514.

867 46. Bansal A, Molina-Cruz A, Brzostowski J, Mu J, Miller LH. 2017. Plasmodium falciparum Calcium-
868 Dependent Protein Kinase 2 Is Critical for Male Gametocyte Exflagellation but Not Essential for
869 Asexual Proliferation. MBio 8.

870 47. Lourido S, Shuman J, Zhang C, Shokat KM, Hui R, Sibley LD. 2010. Calcium-dependent protein
871 kinase 1 is an essential regulator of exocytosis in Toxoplasma. Nature 465:359–362.

872 48. Absalon S, Blomqvist K, Rudlaff RM, DeLano TJ, Pollastri MP, Dvorin JD. 2018. Calcium-
873 Dependent Protein Kinase 5 Is Required for Release of Egress-Specific Organelles in Plasmodium
874 falciparum. MBio 9.

875 49. Sidik SM, Huet D, Ganesan SM, Huynh M-H, Wang T, Nasamu AS, Thiru P, Saeij JPJ, Carruthers

VB, Niles JC, Lourido S. 2016. A Genome-wide CRISPR Screen in Toxoplasma Identifies Essential Apicomplexan Genes. Cell 166:1423–1435.e12.

50. Wernimont AK, Artz JD, Finerty P Jr, Lin Y-H, Amani M, Allali-Hassani A, Senisterra G, Vedadi M, Tempel W, Mackenzie F, Chau I, Lourido S, Sibley LD, Hui R. 2010. Structures of apicomplexan calcium-dependent protein kinases reveal mechanism of activation by calcium. Nat Struct Mol Biol 17:596–601.

51. Sugi T, Kato K, Kobayashi K, Watanabe S, Kurokawa H, Gong H, Pandey K, Takemae H, Akashi H. 2010. Use of the kinase inhibitor analog 1NM-PP1 reveals a role for Toxoplasma gondii CDPK1 in the invasion step. Eukaryot Cell 9:667–670.

52. Bishop AC, Shah K, Liu Y, Witucki L, Kung C, Shokat KM. 1998. Design of allele-specific inhibitors to probe protein kinase signaling. Curr Biol 8:257–266.

53. Garrison E, Treeck M, Ehret E, Butz H, Garbuz T, Oswald BP, Settles M, Boothroyd J, Arrizabalaga G. 2012. A forward genetic screen reveals that calcium-dependent protein kinase 3 regulates egress in Toxoplasma. PLoS Pathog 8:e1003049.

54. Stewart RJ, Whitehead L, Nijagal B, Sleebs BE, Lessene G, McConville MJ, Rogers KL, Tonkin CJ. 2017. Analysis of Ca2+ mediated signaling regulating Toxoplasma infectivity reveals complex relationships between key molecules. Cell Microbiol 19.

55. Shortt E, Lourido S. 2020. Plate-Based Quantification of Stimulated Toxoplasma Egress. Methods Mol Biol 2071:171–186.

56. Sugi T, Kobayashi K, Takemae H, Gong H, Ishiwa A, Murakoshi F, Recuenco FC, Iwanaga T, Horimoto T, Akashi H, Kato K. 2013. Identification of mutations in TgMAPK1 of Toxoplasma gondii conferring resistance to 1NM-PP1. Int J Parasitol Drugs Drug Resist 3:93–101.

57. Long S, Brown KM, Drewry LL, Anthony B, Phan IQH, Sibley LD. 2017. Calmodulin-like proteins localized to the conoid regulate motility and cell invasion by Toxoplasma gondii. PLoS Pathog 13:e1006379.

58. Brown KM, Long S, Sibley LD. 2017. Plasma Membrane Association by N-Acylation Governs PKG Function inToxoplasma gondii. MBio 8:e00375–17.

59. Nishimura K, Fukagawa T, Takisawa H, Kakimoto T, Kanemaki M. 2009. An auxin-based degron system for the rapid depletion of proteins in nonplant cells. Nat Methods 6:917–922.

60. Lourido S, Zhang C, Lopez MS, Tang K, Barks J, Wang Q, Wildman SA, Shokat KM, Sibley LD. 2013. Optimizing small molecule inhibitors of calcium-dependent protein kinase 1 to prevent infection by Toxoplasma gondii. J Med Chem 56:3068–3077.

61. Drewry LL, Sibley LD. 2019. The hitchhiker's guide to parasite dissemination. Cell Microbiol

e13070–15.

62. Leung JM, Rould MA, Konradt C, Hunter CA, Ward GE. 2014. Disruption of TgPHIL1 Alters Specific Parameters of Toxoplasma gondii Motility Measured in a Quantitative, Three-Dimensional Live Motility Assay. PLoS One 9:e85763–10.

63. Gaji RY, Johnson DE, Treeck M, Wang M, Hudmon A, Arrizabalaga G. 2015. Phosphorylation of a Myosin Motor by TgCDPK3 Facilitates Rapid Initiation of Motility during Toxoplasma gondii egress. PLoS Pathog 11:e1005268.

64. Govindasamy K, Bhanot P. 2020. Overlapping and distinct roles of CDPK family members in the pre-erythrocytic stages of the rodent malaria parasite, Plasmodium berghei. PLoS Pathog 16:e1008131.

65. Bansal A, Ojo KK, Mu J, Maly DJ, Van Voorhis WC, Miller LH. 2016. Reduced Activity of Mutant Calcium-Dependent Protein Kinase 1 Is Compensated in Plasmodium falciparum through the Action of Protein Kinase G. MBio 7.

66. Bansal A, Molina-Cruz A, Brzostowski J, Liu P, Luo Y, Gunalan K, Li Y, Ribeiro JMC, Miller LH. 2018. PfCDPK1 is critical for malaria parasite gametogenesis and mosquito infection. Proc Natl Acad Sci U S A 115:774–779.

67. Winterbach W, Van Mieghem P, Reinders M, Wang H, de Ridder D. 2013. Topology of molecular interaction networks. BMC Syst Biol 7:90.

68. Dominicus C, Nofal SD, Broncel M, Kastris NJ, Flynn H, Arrizabalaga G, Botté CY, Invergo BM, Treeck M. 2021. A positive feedback loop mediates crosstalk between calcium, cyclic nucleotide and lipid signalling in Toxoplasma gondii. bioRxiv.

69. Huynh M-H, Carruthers VB. 2006. Toxoplasma MIC2 is a major determinant of invasion and virulence. PLoS Pathog 2:e84.

70. Boucher LE, Bosch J. 2015. The apicomplexan glideosome and adhesins - Structures and function. J Struct Biol 190:93–114.

71. Broncel M, Dominicus C, Vigetti L, Nofal SD, Bartlett EJ, Touquet B, Hunt A, Wallbank BA, Federico S, Matthews S, Young JC, Tate EW, Tardieux I, Treeck M. 2020. Profiling of myristoylation in Toxoplasma gondii reveals an N-myristoylated protein important for host cell penetration. Elife 9.

72. Foe IT, Child MA, Majmudar JD, Krishnamurthy S, van der Linden WA, Ward GE, Martin BR, Bogyo M. 2015. Global Analysis of Palmitoylated Proteins in Toxoplasma gondii. Cell Host Microbe 18:501–511.

73. Amos B, Aurrecoechea C, Barba M, Barreto A, Basenko EY, Bażant W, Belnap R, Blevins AS,

Böhme U, Brestelli J, Brunk BP, Caddick M, Callan D, Campbell L, Christensen MB, Christophides GK, Crouch K, Davis K, DeBarry J, Doherty R, Duan Y, Dunn M, Falke D, Fisher S, Flicek P, Fox B, Gajria B, Giraldo-Calderón GI, Harb OS, Harper E, Hertz-Fowler C, Hickman MJ, Howington C, Hu S, Humphrey J, Iodice J, Jones A, Judkins J, Kelly SA, Kissinger JC, Kwon DK, Lamoureux K, Lawson D, Li W, Lies K, Lodha D, Long J, MacCallum RM, Maslen G, McDowell MA, Nabrzyski J, Roos DS, Rund SSC, Schulman SW, Shanmugasundram A, Sitnik V, Spruill D, Starns D, Stoeckert CJ, Tomko SS, Wang H, Warrenfeltz S, Wieck R, Wilkinson PA, Xu L, Zheng J. 2022. VEuPathDB: the eukaryotic pathogen, vector and host bioinformatics resource center. Nucleic Acids Res 50:D898–D911.

74. Ishino T, Orito Y, Chinzei Y, Yuda M. 2006. A calcium-dependent protein kinase regulates Plasmodium ookinete access to the midgut epithelial cell. Mol Microbiol 59:1175–1184.

75. Gurnett AM, Liberator PA, Dulski PM, Salowe SP, Donald RGK, Anderson JW, Wiltsie J, Diaz CA, Harris G, Chang B, Darkin-Rattray SJ, Nare B, Crumley T, Blum PS, Misura AS, Tamas T, Sardana MK, Yuan J, Biftu T, Schmatz DM. 2002. Purification and molecular characterization of cGMP-dependent protein kinase from Apicomplexan parasites. A novel chemotherapeutic target. J Biol Chem 277:15913–15922.

76. Bastin P, Bagherzadeh Z, Matthews KR, Gull K. 1996. A novel epitope tag system to study protein targeting and organelle biogenesis in Trypanosoma brucei. Mol Biochem Parasitol 77:235–239.

77. Dobrowolski JM, Carruthers VB, Sibley LD. 1997. Participation of myosin in gliding motility and host cell invasion by Toxoplasma gondii. Mol Microbiol 26:163–173.

78. Starnes GL, Jewett TJ, Carruthers VB, Sibley LD. 2006. Two separate, conserved acidic amino acid domains within the Toxoplasma gondii MIC2 cytoplasmic tail are required for parasite survival. J Biol Chem 281:30745–30754.

79. Waldman BS, Schwarz D, Wadsworth MH 2nd, Saeij JP, Shalek AK, Lourido S. 2020. Identification of a Master Regulator of Differentiation in Toxoplasma. Cell 180:359–372.e16.

80. Burg JL, Perelman D, Kasper LH, Ware PL, Boothroyd JC. 1988. Molecular analysis of the gene encoding the major surface antigen of Toxoplasma gondii. J Immunol 141:3584–3591.

81. Plattner F, Yarovinsky F, Romero S, Didry D, Carlier M-F, Sher A, Soldati-Favre D. 2008. Toxoplasma profilin is essential for host cell invasion and TLR11-dependent induction of an interleukin-12 response. Cell Host Microbe 3:77–87.